Chinese Chemical Letters 36 (2025) 109997

Contents lists available at ScienceDirect

Chinese Chemical Letters

journal homepage: www.elsevier.com/locate/cclet

Research progress of modified metal current collectors in sodium metal anodes

Zhenyang Yu[a,*], Yueyue Gu[a], Qi Sun[a], Yang Zheng[a], Yifang Zhang[b,*], Mengmeng Zhang[b], Delin Zhang[c,d], Zhijia Zhang[b,c,e,*], Yong Jiang[b,c]

[a] School of Mechanical Engineering, Tiangong University, Tianjin 300387, China
[b] School of Material Science and Engineering, State Key Laboratory of Separation Membrane and Membrane Processes, Tiangong University, Tianjin 300387, China
[c] School of Electronic and Information Engineering, Institute of Quantum Materials and Devices, Tiangong University, Tianjin 300387, China
[d] Cangzhou Institute of Tiangong University, Cangzhou 061000, China
[e] Jiangsu Fuyuan Mustard Seed Space New Material Research Institute Co., Ltd., Xuzhou 221000, China

ARTICLE INFO

Article history:
Received 6 March 2024
Revised 29 March 2024
Accepted 10 May 2024
Available online 11 May 2024

Keywords:
Sodium metal anodes
Metal current collector
Surface modification
Surface structural design
Anode-free batteries

ABSTRACT

Sodium metal has been widely studied in the field of batteries due to its high theoretical specific capacity (~1,166 mAh/g), low redox potential (-2.71 V compared to standard hydrogen electrode), and low-cost advantages. However, problems such as unstable solid electrolyte interface (SEI), uncontrolled dendrite growth, and side reactions between solid-liquid interfaces have hindered the practical application of sodium metal anodes (SMAs). Currently, lots of strategies have been developed to achieve stabilized sodium metal anodes. Among these strategies, modified metal current collectors (MCCs) stand out due to their unique role in accommodating volumetric fluctuations with superior structure, lowering the energy barrier for sodium nucleation, and providing guided uniform sodium deposition. In this review, we first introduced three common metal-based current collectors applied to SMAs. Then, we summarized strategies to improve sodium deposition behavior by optimally engineering the surface of MCCs, including surface loading, surface structural design, and surface engineering for functional modification. We have followed the latest research progress and summarized surface optimization cases on different MCCs and their applications in battery systems.

1. Introduction

Due to the gradual depletion of non-renewable resources, such as fossil energy, and the realistic demand for new and clean energy in modern society, the importance of high-energy-density energy storage devices is becoming increasingly prominent [1-5]. Rechargeable batteries, as an energy storage device with great potential, have attracted extensive attention and research [6-8]. Although lithium-ion batteries (LIBs) have a wide range of applications in electric vehicles, portable devices and other fields, the further improvement of their energy density faces a bottleneck owing to the limitation of positive and negative electrode capacity [9-11]. Alkali metals have become the preferred materials for the anode of secondary batteries due to their high theoretical specific capacity and low redox potential [12,13]. Among the available alkali metal materials (Na, Li, and K), sodium is abundant and widely distributed in natural resources, and possesses a great cost advantage in the development of materials and application of batteries (Table 1) [14,15]. Sodium metal has a high theoretical specific capacity (~1166 mAh/g) and low redox potential, and has similar physical and chemical properties to lithium, so it is expected to be the anode material for a new generation of high-performance batteries [16].

The research on innovative technologies related to sodium metal batteries (SMBs) is in full swing. However, sodium metal with high reactivity readily reacts with the electrolyte to form a solid electrolyte interface (SEI) at the interface [17,18]. During the plating/stripping of the sodium metal, the inhomogeneous sodium deposition would cause the electrode volume to change dramatically, thus causing the SEI film to continuously rupture and regenerate. This process continuously depletes the limited sodium metal and electrolyte, decreasing the Coulombic efficiency (CE) of the battery and ultimately impairing the cycle lifespan [19,20]. In addition, uneven sodium deposition results in the growth of sodium

* Corresponding authors.
E-mail addresses: yuzhenyang@tiangong.edu.cn (Z. Yu), zhangyifang@tiangong.edu.cn (Y. Zhang), zhangzhijia@tiangong.edu.cn (Z. Zhang).

https://doi.org/10.1016/j.cclet.2024.109997
1001-8417/

Table 1
Comparison of physical and chemical properties of Na, Li, and K.

Parameter	Na	Li	K
Density (g/cm^3)	0.968	0.534	0.862
Relative atomic mass	22.98	6.941	39.089
Voltage (V) *vs.* SHE	−2.71	−3.04	−2.93
Ionic radium (Å)	1.02	0.76	1.38
Theoretical specific capacity (mAh/g)	1166	3860	687
Content in Earth's crust (%)	2.74	0.0065	2.47

dendrites, which may puncture the diaphragm and trigger an internal short circuit in the battery, thus creating a serious safety issue [21,22].

With the aim of further promoting high-energy-density battery technology with high portability and safety, the concept of "anode-free sodium metal batteries" (AFSMBs) has been developed [23-25]. This battery is unique in that it does not have an additional metal anode, but rather utilizes sodium metal deposited on the current collector by the cathode as the anode. This design not only reduces the total weight of the battery, but also significantly enhances the safety of the battery system because the deposition process of the sodium metal occurs inside the closed cell. An innovative and promising path to the development of high-energy-density battery systems is provided by this. However, the design of AFSMBs has similar challenges to those of metal batteries, such as the higher overpotential of sodium nucleation on the current collector leading to inhomogeneity of metal deposition, and the solid-liquid interfacial parasitic reactions become more serious [26-28]. The limited source of sodium is depleted in cycles with little reversibility, ultimately leading to battery failure. Therefore, ensuring the uniform deposition of sodium metal with high CE on the current collector remains a core challenge for realizing high-energy-density SMBs.

In order to realize high-performance SMBs, researchers have put a deal of effort into the following three areas: (1) Optimization of the electrolyte system [29-31]. The components, concentration and additives of the electrolyte are carefully formulated with the aim of reducing side reactions and forming a stable and robust SEI film on the sodium metal surface. (2) Construction of artificial SEI [32-34]. Physical, chemical, and electrochemical methods are employed to create an artificial protective layer, which not only enhances the ion transport capacity of the SEI membrane, but also its mechanical rigidity. (3) Current collector modification [35-38]. The sodium deposition behavior on the current collector surface was improved by constructing a sodium-friendly layer and designing a three-dimensional (3D) structure, which effectively inhibited the growth of dendrites. Among numerous alternative materials, metal current collectors (MCCs) are the most widely used because of their simple manufacturing process and low prices. The geometry and surface properties of MCCs directly impact the sodium deposition behavior during the circulation process, and modification of the MCCs could be a radical solution to the flaws of sodium deposition.

In this review, we summarized the strategies for the modification of MCCs from three aspects, one is to load a protective layer on the surface of the planar MCCs, which enhances the sodium affinity of the substrate, reduces the energy barriers for the nucleation of metallic sodium, and improves the deposition behavior of sodium. The second one is to construct MCCs with 3D structure. The large specific surface area of the 3D skeleton could provide more nucleation sites for sodium, reduce the local current density, facilitate the uniform distribution of ions, and alleviate the volume expansion of the electrode to some extent. In addition, functional MCCs could be fabricated to scheme the deposition route of sodium and avoid dendrites through unique structural design and the introduction of magnetic elements. We introduced the latest research results and gained an understanding of the latest research trends in MCCs engineering. We hope that this review can provide some convenience for scholars' research and contribute to the development of secondary batteries.

2. Classification of MCCs

The current collector is an indispensable component of a battery. It can not only carry the active material but also collect and output the current generated by the active electrode material [39]. In principle, ideal current collectors should meet the following conditions: (1) High conductivity; (2) satisfactory chemical and electrochemical stability; (3) high mechanical strength; (4) excellent compatibility and bonding with electrode active substances; (5) cheap and easy to obtain; (6) lightweight. In the following, we briefly introduce the metal-based current collectors applied in SMBs from the point of view of different materials.

2.1. Copper-based current collectors

Copper (Cu) is an excellent metal conductor with electrical conductivity second only to silver, with high electrical conductivity, high ductility and many other advantages. Common copper–based current collectors include Cu foil, Cu foam and Cu mesh.

Electrolytic Cu foil is widely used in the preparation of sodium and lithium batteries owing to its important advantages in electrical conductivity, mechanical strength and low coefficient of thermal expansion [40,41]. However, the production and manufacturing process inevitably leaves peripheral defects on the surface of Cu foil, which are not conducive to uniform ion distribution during the electrochemical process. Moreover, at high potentials, Cu foil is easily oxidized, which could impose certain limitations on the performance of batteries [42,43].

Cu foam is a 3D mesh material similar to a sponge, which has many advantages such as high electrical conductivity, high thermal conductivity, and large specific surface area. Due to these unique properties, Cu foam has a wide range of applications in many fields. In the field of batteries, copper foam can be used as electrode skeleton material, which can provide sufficient structural support and improve the stability of the electrode [44,45]. When used in metal batteries, Cu foam can effectively inhibit the volume change of the electrode during the charging and discharging process and slow down the phenomenon of dendrites, thus improving the charging and discharging performance of the battery [46-48].

2.2. Aluminum-based current collectors

Aluminum (Al) has good electrical conductivity, although not as good as copper, but its density is lower (2.7 g/cm^3), and the resource of aluminum is abundant. According to preliminary calculations, the storage of aluminum deposits accounts for about 8% or more of the constituent materials of the earth's crust.

The use of Al foil as the current collector is conducive to improving the weight energy density and economic efficiency of batteries. However, Al foil is susceptible to localized corrosion due to electrochemical oxidation with solvent molecules of the electrolyte at higher potentials, which may lead to barriers such as increased internal resistance and reduced battery lifespan [49,50].

Al foam with a pore structure has a complex and costly production process, and its application in batteries is not widespread. However, researchers have applied it to LIBs and achieved high power density and energy density, so it is also a current collector with great potential [51,52]. In order to achieve the goal of high-performance batteries, new aluminum-based composite current collector materials with high stability and cost efficiency need to be investigated in more detail.

2.3. Nickel-based current collectors

Nickel (Ni) is equipped with excellent corrosion resistance and thermal stability, which make it one of the ideal choices for battery current collectors. There are two main types of nickel-based current collectors: Ni foam and Ni foil. Currently, researchers are actively studying the application of nickel foil in ion-batteries, but due to the relatively smooth surface of nickel foil, the active material tends to separate from the collector during long-term cycling [53,54]. In order to enhance the bonding of both, surface pretreatment is usually required.

In addition, nickel foam possesses a 3D skeleton structure, which not only increases the contact area with the active material, but also reduces the contact resistance between the active material and the collector. Although the application of nickel-based current collectors on SMAs is not yet common, the results of the existing studies show that they have great potential and are subject to further research and development in the future.

2.4. Other metallic current collectors

Except for the MCCs mentioned above, there are some unusual metal-based current collectors that have been applied to SMAs [55,56]. For example, stainless steel (SS) foils offer corrosion resistance and easy recyclability, as well as high strength and large-scale production. However, SS foils fail to have a sufficient affinity for sodium, and thus suffer from a host of challenges in sodium electrode applications, such as high contact resistance.

3. Surface modification engineering of MCCs

3.1. Surface loading based on planar MCCs

Since the geometry and surface chemistry of planar MCCs affect the battery performance such as internal resistance and cycle stability, constructing a passivation layer on the surface of metal collectors is a simple and efficient strategy. Next, we will summarize the modification methods of planar MCCs in terms of surface coating and *in-situ* synthesis.

3.1.1. Coating on the flat surface

The simple surface loading process is a widely used modification strategy because versatile coating materials can be introduced directly into the substrate without changing the morphology of the MCCs. Carbon-based materials are widely used as coating materials thanks to their light mass, high conductivity and corrosion resistance [57,58]. For example, the popularity of commercially available carbon-coated Cu (Al) foil demonstrates the potential for large-scale production and application. O.J. Dahunsi *et al.* assembled cells using battery-grade Al foil and carbon-coated Al foil (C@Al) to evaluate the influence of carbon coating on the sodium plating/stripping process (Fig. 1a) [59]. To ensure the consistency of the experiments, they set a constant plating capacity of 3 mAh/cm^2 and an ether-based electrolyte of 30 μL/cell. The experimental results showed that the C@Al exhibited lower overpotentials and more stable voltage distributions at different current densities ranging from 0.5 mA/cm^2 to 3 mA/cm^2. In particular, at a current density of 3.0 mA/cm^2, the overpotential of the C@Al around 100 mV, which was only one-third of that of the bare Al foil under the same conditions (Fig. 1b). Through a series of tests and characterizations, it was successfully demonstrated that the C-Al junction interfaces could effectively regulate the plating/stripping behavior of sodium. Moreover, further research is needed to rationalize the introduction of the abundance of coating materials and to ensure their viability in battery systems.

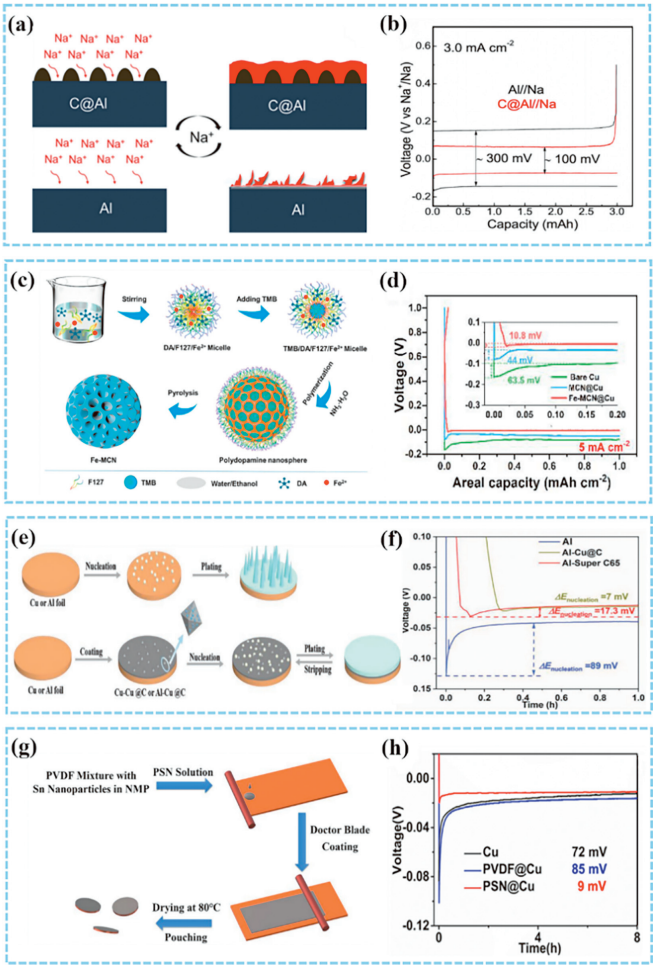

Fig. 1. (a) Schematic illustration of Na plating. (b) Voltage profiles for Na plating and striping at 3 mA/cm^2. Reproduced with permission [59]. Copyright 2023, American Chemical Society. (c) Schematic diagram of the synthesis process of Fe-MCNs. (d) Comparison of nucleation overpotentials of different current collectors at 5 mA/cm^2 and 1 mAh/cm^2. Reproduced with permission [60]. Copyright 2022, American Chemical Society. (e) Schematics of Na deposition on different current collectors. (f) Nucleation overpotentials of substrates at 1 mA/cm^2. Reproduced with permission [61]. Copyright 2022, Wiley-VCH GmbH. (g) Schematic diagram for the preparation of PSN@Cu. (h) Comparison of nucleation overpotentials of different current collectors at 0.5 mA/cm^2 and 4 mAh/cm^2. Reproduced with permission [63]. Copyright 2020, American Chemical Society.

An atomically dispersed Fe-doped mesoporous carbon nanospheres (Fe-MCN) were designed and then coated on Cu foils to prepare modified current collectors by Wei *et al.* (Fig. 1c) [60]. At a high current density of 5 mA/cm^2, the nucleation overpotential of Fe-MCN modified Cu substrate (Fe-MCN@Cu) is only 10.8 mV, significantly lower than that of bare Cu foil (44.5 mV), indicating that Fe-MCN effectively enhances the affinity of the substrate for Na (Fig. 1d). The atomically dispersed Fe doped in the mesoporous carbon results in a more uniform distribution of sodium nucleation sites, which facilitates the uniform deposition of Na. In addition, carbon nanospheres promote rapid charge transfer between electrons and Na ions due to their uniform mesoporous structure and large specific surface area. Benefiting from the above advantages, the modified Cu substrates exhibit excellent electrochemical performance at 1 mA/cm^2 and 1 mAh/cm^2: The CE of the half-cell is as high as 99.97% in 850 cycles, and symmetric cell using Fe-MCN@Cu electrodes pre-deposited with 6 mAh/cm^2 exhibits excellent cycle life of up to 2500 h and small voltage hysteresis of only 9 mV.

In addition, Li's team prepared an active material with copper nanoparticles embedded in a carbon framework using copper

nitrate trihydrate as the copper source and polyvinyl pyrrolidone (PVP) as the precursor nanofiber [61]. Applying this composite to conventional MCCs can form a strong nucleation buffer layer (denoted as Cu-Cu@C and Al-Cu@C). The addition of copper nanoparticles draws ample active sites for Na ions, and the robust 3D carbon skeleton provides pore volume for the battery to minimize the volume change during plating/stripping (Fig. 1e). The initial Na nucleation overpotentials of bare Al and Al-Cu@C were 89 and 7 mV, when using an ether electrolyte at a current density of 1 mA/cm^2 (Fig. 1f). The comparison of the data indicates that the incorporation of Cu@C composites effectively reduces the nucleation barriers for Na plating on the Cu and Al foils. *In situ* dilatometry investigation was used to study the volume change of the cell during the first three cycles. Due to the accumulation of inactive sodium during the cycling process, the Cu foil exhibited irreversible thickness expansion. In contrast, the change in electrode thickness of Cu-Cu@C during cycling is only 10 μm, and the accumulation of inactive sodium is almost insignificant.

Polyvinylidene difluoride (PVDF) is often used as a binder for composite electrodes due to its superior abrasion and corrosion resistance. Hou *et al*. constructed a PVDF layer on Cu foil by a common doctor blade coating technique [62]. The cell assembled with PVDF@Cu as the electrode has a stable cycle life of 1200 h at a current density of 1 mA/cm^2. However, the low mechanical modulus and ion diffusion conductivity of the PVDF binder were insufficient for an ideal battery configuration [63]. Chen *et al*. introduced appropriate Sn nanoparticles into a PVDF matrix and successfully scraped and coated an organic-inorganic composite protective layer with a thickness of about 2.63 μm on Cu foil (PSN@Cu). The Young's modulus of the protective layer with Sn nanoparticles reached 5.48 GPa, which is much higher than that of the polymer-only layer (Fig. 1g). Moreover, the PSN@Cu achieved a tiny voltage hysteresis (9 mV) at 0.5 mA/cm^2 and 4 mAh/cm^2 than that of the bare Cu (Fig. 1h).

Wang *et al*. constructed a peelable organic/inorganic protective layer by uniformly coating a mixed slurry containing NaF particles and PVDF polymers onto Al foils [64]. They observed different substrates deposited with 0.5 mAh/cm^2 sodium by scanning electron microscopy (SEM) and found that there were many needle-like sodium dendrites with sizes ranging from 1 μm to 10 μm on the surface of the bare Al foil, which could lead to short-circuiting of the battery. Surprisingly, on the surface of the Al foil loaded with an organic/inorganic protective layer, a complete and smooth film without any visible sodium dendrites was obtained.

The introduction of modified materials could improve the affinity between the substrate and sodium, decrease the nucleation barrier of sodium, and optimize the cycling performance of the battery. Currently, widely used coating materials include carbon-based materials, organic materials, hybrid organic/inorganic hybrid materials, and nanoscale sodiophilic metals. However, in order to further improve the battery performance, optimizing the physical properties of the coating materials as well as ensuring their structural integrity during long cycling still requires in-depth research. In addition, considering the high cost of superior composite carbon materials, the irreversible reaction of organic coating materials with sodium, and the poor application of hybrid organic/inorganic coating materials in SMBs, the research and development of selecting superior coating materials that are both low-cost and industrially scalable for sodium batteries still requires enhancement.

3.1.2. In-situ synthesis sodiophilic layer

In addition to using the doctor-blade method to introduce the coating directly onto the surface of planar MCCs, it is also possible to synthesize the layer *in situ* on their surfaces by chemical/electrochemical reactions. Wu *et al*. optimized the crystal orientation and surface properties of a 20 μm thick commercial Al foil by annealing and fluorination [65]. The binding energies of Na atoms adsorbed on different planes were calculated using density functional theory (DFT). It was found that the binding energies of sodium atoms on oxidized Al and fluorinated Al (F-A-Al) were −1.54 and −2.02 eV, respectively. The lower binding energies showed that the annealing and fluorination treatments enhanced the sodium affinity of the Al foil surface, which was beneficial for guiding the homogeneous deposition of sodium metal (Fig. 2a). Optical observation and depth composition images also show that the surface texture of Na deposited on the F-A-Al electrode is smooth and regular in shape. Excess Na metal (2 mAh/cm^2) was deposited in the initial stage and then repeating the plating/stripping cycles at 0.5 mA/cm^2 and 0.5 mAh/cm^2, F-A-Al achieved more than 300 stable cycles (Fig. 2b). Furthermore, the anode-free full cell equipped with an F-A-Al current collector, $Na_3V_2(PO_4)_3$ (NVP) cathode, and high-temperature (90 °C) ionic liquid electrolyte obtained a high initial CE during cycling and demonstrated a high energy density. The anode-free full cells with a high mass loading of NVP cathode (∼11.3 mg/cm^2) maintain a 98% capacity retention after 50 cycles. These findings portend a promising future for modified metal current collector design in high-energy-density battery applications.

Moreover, Zhu *et al*. prepared CuP_2 particles through high-temperature solid/gas state reactions and successfully converted them into Cu and Na_3P hybrid nanoparticles by utilizing *in-situ* electrochemical sodiation reactions [66]. These hybrid nanoparticles formed a mixed ion/electronic conductive interface (MIECI) layer on the surface of the Cu foil (Fig. 2c). The half-cell was assembled with CuP_2@Cu foil (Cu foil) as the working electrode and Na foil as the counter electrode. Promisingly, the Na||CuP_2@Cu cell was able to cycle stably for over 700 cycles at 1 mA/cm^2 and 1 mAh/cm^2, with an average CE of 99.81%. In contrast, the Na||Cu cell was highly unstable and exhibited micro-short circuit, indicating that the plating/stripping of Na on CuP_2@Cu has more excellent kinetics. The *in-situ* generation of the MIECI layer significantly improved the affinity of the current collector to the deposited Na, leading to the homogenization of the Na^+ flux. In addition, by pre-depositing a certain amount of Na on CuP_2@Cu foil and coupling it with a highly loaded $NaTi_2(PO_4)_3$ cathode, the full cell with a negative to positive electrode (N/P) capacity ratio of about 4 exhibits excellent stability at 5 C, and its performance remains stable even after 800 cycles (Fig. 2d).

Wang *et al*. constructed ordered molecular layers containing coordinating formate ligands on the Cu (110) surface by a simple hydrothermal method [67]. During the initial deposition process, the formate ligand present on the modified-Cu surface was capable of spontaneously transforming into sodium formate (HCOONa). The HCOONa interface boasts high chemical stability and a low diffusion barrier for Na ions, while its structural order and compactness surpass those of most organic SEI components. Optical images of *in-situ* deposited sodium at a current density of 3 mA/cm^2 show that the HCOONa-modified current collector surface remains flat and bubble-free even after 120 min of plating. This demonstrates that the HCOONa interface can effectively guide dendrite-free Na plating and inhibit parasitic reactions between sodium anode and electrolyte.

The researchers also deposited sodiophilic metal particles on the MCCs surface by magnetron sputtering [68,69], electrodeposition [70], and electron-beam evaporation [71] in order to construct an *in-situ* sodium-friendly alloy surface. Tang's team sputtered an ultrathin layer of Au on the surface of Cu foil and successfully introduced a sodiophilic Au-Na alloy layer through the alloying reaction in the initial cycle [68]. The chemical structure of the surface layer of the current collector after the first cycle was examined using X-ray diffraction (XRD), and some alloying phases or layers were found which is proved by the alloy phase Au_2Na

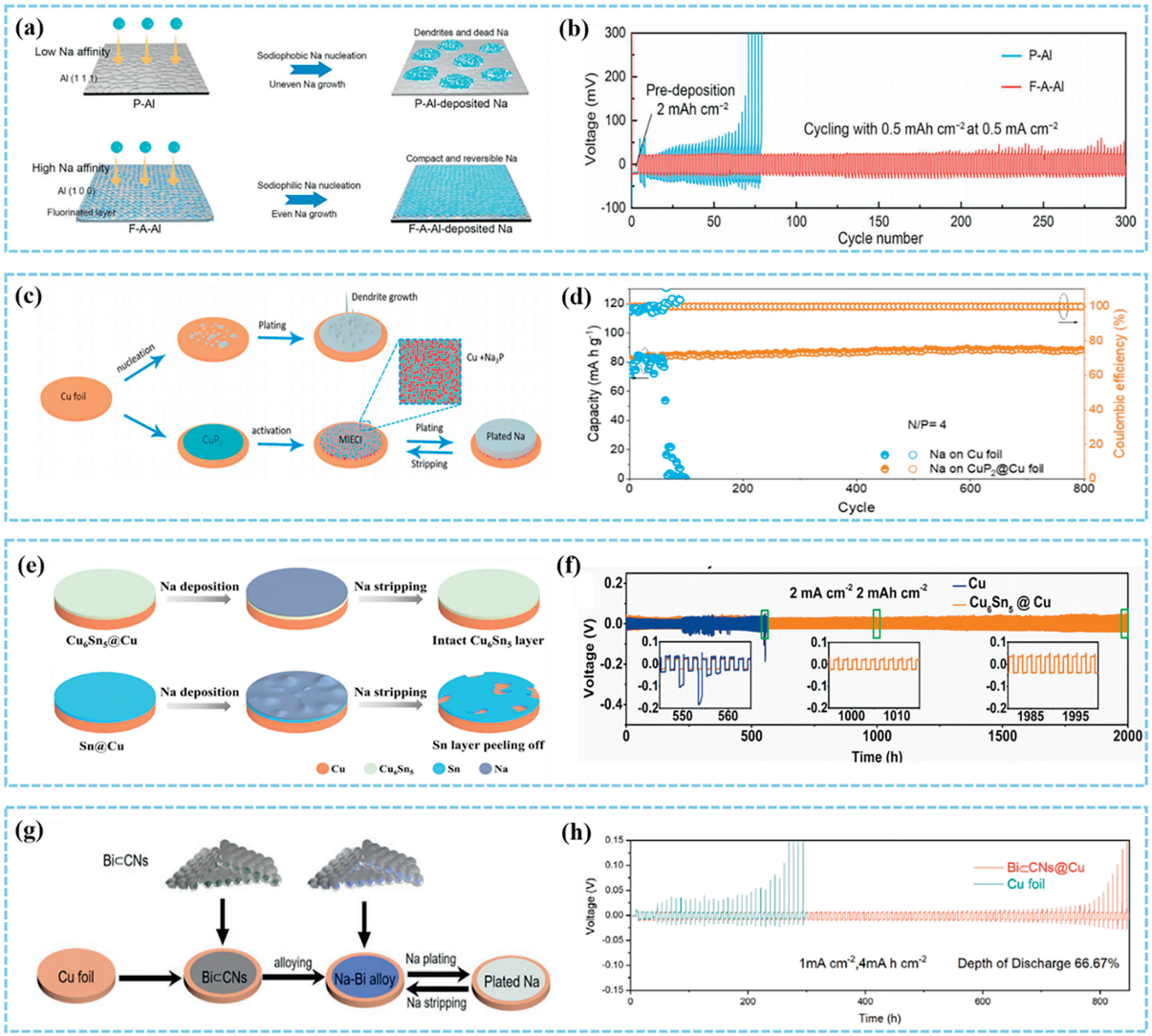

Fig. 2. (a) Schematic illustration of Na plating on different current collectors. (b) Voltage profiles for Na plating and striping at 0.5 mA/cm^2 and 0.5 mAh/cm^2. Reproduced with permission [65]. Copyright 2023, Wiley-VCH GmbH. (c) Schematic illustration of Na plating. (d) Cycling performance of the full cells at 5 C. Reproduced with permission [66]. Copyright 2022, Elsevier. (e) Schematic illustration of Na plating. (f) Cycling performance of symmetrical cells at 2 mA/cm^2 and 2 mAh/cm^2. Reproduced with permission [70]. Copyright 2021, Elsevier. (g) Schematics of Na deposition. (h) Voltage profiles of sodium plating/stripping on the bare Cu foils and Bi⊂CNs@Cu. Reproduced with permission [72]. Copyright 2021, Wiley-VCH GmbH.

shown in the pattern. The Au-Na alloy layer supplies more nucleation sites for the deposition of Na, which contributes to forming a uniform and dense Na layer.

However, owing to the pricey concern of Au, it is not very suitable for large-scale practical production applications. Tang and colleagues had successfully identified affordable metals that may be used to replace Au. By using magnetron sputtering to deposit various metals onto Cu foil, they discovered that tin (Sn) and antimony (Sb) could also be *in-situ* alloyed during the initial cycle [69]. The test results show that sodium has a low nucleation overpotential when Au, Sn, and Sb are used as substrates, and the nucleation overpotential does not increase significantly with increasing current density. Meanwhile, the good permeability with molten sodium implies the potential of Sn and Sb as low-cost metal substitutes for Au.

Chen *et al*. constructed the Cu_6Sn_5 alloy layer on commercial Cu foil measuring 850 mm × 650 mm by a simple chemical tin plating method and compared it with the case of tin-coated Cu foil using the electro-deposition process [70]. The Sn element in the alloy layer reduces the nucleation barrier of Na, and the Cu element acts as a mechanical buffer to alleviate the internal stress (Fig. 2e). Due to these synergistic effects, the Cu_6Sn_5 alloy-coated Cu foil exhibits an impressive life extension of up to 2000 cycles at ultra-high discharge depths (50%), whereas the Cu collector showed voltage oscillations after 300 h and finally failed at 550 h (Fig. 2f). Furthermore, when paired with the FeS_2 cathode, the full cell has managed to operate stably for 1500 cycles with a striking 95% capacity retention.

Zhang *et al*. proposed carbon nanosheets embedded with Bi nanoparticles (NPs) to construct a robust buffer layer on the surface of Cu foils (denoted as Bi⊂CNs@Cu) [72]. The Bi NPs allow the *in-situ* formation of sodiophilic Na-Bi alloy, which can effectively reduce the nucleation barriers for the deposition of Na metal (Fig. 2g). The large surface area of carbon nanosheets supplies more sodium nucleation sites and ensures the uniform deposition of sodium metal in the subsequent stages. This results in the excellent electrochemical performance of the battery using Bi⊂CNs@Cu as current collectors in terms of CE and cycling stability. The half-cell can be continuously cycled for nearly 7700 h (1287 cycles) at a high face capacity of 3 mAh/cm^2 with an average CE of 99.92%.

The symmetric cell could sustain more than 850 h at a depth of discharge of up to 66.67% (Fig. 2h).

Both the catalytic current collector surface and the introduction of a sodiophilic metal could construct an *in-situ* sodiophilic layer on the MCCs surface, thus effectively regulating the nucleation behavior of sodium. However, the preparation and use of catalysts are limited by the fabrication process, production cost, and reaction conditions; the addition of alloy layers increases the weight of the cell thereby impairing the energy density of the battery. Indeed, the investigation and discovery of low-cost and high-quality catalysts for modified MCCs surface, as well as the optimization of the rational spatial arrangement of the pro-sodium layer, are both essential for the further development of SMAs.

3.2. Design of surface structure

The 3D framework could effectively inhibit the growth of sodium dendrites by reducing the local current density and enhancing the deposition nucleation sites of sodium. In addition, 3D MCCs provide sufficient buffer space for the volume change of the electrode during plating and stripping due to its large specific surface area and porosity. In this section, we summarized the recent research progress in the field of SMBs with 3D structural design of flat MCCs and surface optimization of 3D MCCs.

3.2.1. 3D structural design of planar MCCs

Micrometer-scale protrusions and pits inevitably exist on flat metal foil surfaces. These rough sites have uneven current density distribution and are prone to form dendritic or moss-like dendrites during sodium plating. Constructing a 3D structure on the surface of a planar MCC with lower production costs is also a simple and efficient modification method [73]. Liu *et al*. used an electrochemical etching strategy to transform commercial flat Al foil into 3D porous Al with abundant cross-linked pores on the surface (Figs. 3a and b). Compared with the instability and short cycle life of Al foil at 0.25 mA/cm^2 in the ester-based electrolyte, it has excellent long-term stability (Fig. 3c). In an anode-free full cell, by using porous Al as the current collector for anode and TiS_2 as the cathode, a stable operation was achieved for 200 cycles at a current density of 0.1 mA/cm^2.

Similarly, Tang *et al*. successfully prepared a 3D skeleton composed of interconnected Al nanosheet arrays (Al NSARs) by etching commercial Al foil (Fig. 3d) [74]. The interlinked Al-NSARs were able to increase the nucleation surface of sodium, thereby decreasing the flux distribution of Na^+ and contributing to the improvement of the reversible sodium plating/stripping behavior (Fig. 3e). The symmetric cells were assembled by depositing sodium with a capacity of 2 mAh/cm^2 on bare Al foil and Al NSARs paired with an ether-based electrolyte. At an area capacity of 1 mAh/cm^2 and a current density of 1 mA/cm^2, the sodium plating/stripping of the Al NSARs was more stable and could be cycled for more than 750 h with low voltage hysteresis ~20 mV (Fig. 3f). On the contrary, the voltage polarization based on bare Al foil started to increase abruptly at 260 h, and the battery was short-circuited after 320 h Al-NSARs provide a greatly effective strategy for the development of practical MCCs, which are helpful in improving cell performance and reducing cost.

In addition to electro-etching the current collector to obtain a 3D structure, it is also possible to deposit a 3D structure of another material on its surface. Xu *et al*. synthesized honeycomb-like hierarchical 3D porous nickel skeletons on planar Cu foils using a rapid and efficient hydrogen bubble dynamic template (HBDT) electro-deposition technique [75]. The mechanism of sodium plating on porous nickel frameworks is revealed by observing the morphological evolution of sodium deposition on 3D current collectors (Figs. 3g and h). Sodium initially nucleates in the vertical pores of the honeycomb-like structure and gradually spreads to the horizontal direction with increasing capacity. Eventually, the deposited layer vertically stacks throughout the honeycomb pores and forms a smooth metal layer on the surface, achieving uniform sodium deposition without dendrites. Although the nickel in the 3D Ni@Cu current collector constitutes a certain volume of the cell, the sodium deposition is able to fill its honeycomb structure sufficiently so that it does not diminish the volumetric energy density of the battery. Thanks to its unique 3D conductive scaffold structural feature, the battery can achieve highly stable cycling performance (Fig. 3i).

In the study of Cai *et al*., magnetron sputtering was used to deposit a 3D Zn nanofibrous layer onto an Al foil (3D Zn@Al), resulting in a thickness of approximately 1.6 μm and a fiber diameter ranging between 100 nm and 150 nm [76]. Finite element analysis simulating the electric field distribution proved that bare Al tends to form dendrites due to the tip effect at the plating stage, while 3D Zn@Al collector can redistribute the electric field, uniform charge dispersion, and guide the uniform deposition of sodium. Compared to the Al/Na anode (1.9 mA/cm^2), the 3D Zn@Al/Na anode exhibited a higher exchange current density (2.7 mA/cm^2), which indicates the excellent Na^+ diffusion kinetics of the 3D Zn@Al/Na anode. The contact angle of 3D Zn@Al with 1 mol/L $NaPF_6$ in 1,2-dimethoxyethane (DME) electrolyte was 11°, significantly smaller than that of 39° for Al foil, demonstrating that the nanofiber-like Zn coating improved the wettability of the electrolyte. Thanks to the high sodiophilicity and uniform electric field distribution of the 3D Zn@Al collector, the Zn@Al/Na||NVP full cell has excellent cycling stability (98.11% capacity retention after 2000 cycles at 50 C). Most notably, the anode-free full cell using NVP as the cathode exhibits excellent cycle life, with a capacity retention rate of 98.8% after 100 cycles.

Similarly, Lu *et al*. fabricated 3D Cu nanowires with a diameter of 40 nm by rearranging copper on the surface of commercial Cu foil *via* hydrothermal method [77]. The prepared 3D Cu nanowires were characterized by large open space, high conductivity, and fine diameter (Figs. 3j and k). In contrast to the Cu foil, which showed short-circuiting after 180 h, the 3D Cu nanowires exhibited a more stable electrochemical cycling behavior, and the voltage distribution remained good after cycling for more than 250 h at 0.5 mA/cm^2 (Fig. 3l). This is attributed to the fact that the skeleton of 3D porous nanowires has many sites acting as charge centers, which greatly homogenizes the ionic flux and reduces the inhomogeneity of charge distribution, thus promoting uniform plating of Na. Soft-packaged full batteries were assembled with $Na_3V_2(PO_4)_3$@C as the cathode and 1 mAh/cm^2 Na-deposited 3D Cu as the anode could be stably cycled for more than 200 cycles with a reversible capacity of 91.7 mAh/g at 0.5 C.

3.2.2. Surface structure optimization of 3D MCCs

An excessively rich pore structure and a large specific surface area can subconsciously consume a considerable amount of electrolyte, leading to the formation of excess SEI, which can somewhat reduce the battery's cycle life. Furthermore, it will also heighten the diffusion barrier of sodium ions, resulting in irreversible sodium loss. Therefore, it is necessary to optimize the surface structure of 3D MCCs to improve battery performance. Shuai *et al*. utilized the chemical reaction of Al and Al_2O_3 with hydrogen fluoride (HF) to fluorinate the Al foam, followed by immersing the HF-treated Al foam into molten sodium to prepare composite electrodes [78]. The symmetric cell assembled with this composite electrode operated stably at 2 mA/cm^2 and 2 mAh/cm^2 for more than 2200 h.

Similarly, Wang's team treated the porous Cu foam by simple oxidation/sulfidation methods, which created a 3D porous core-shell cylindrical structure with copper oxide (or sulfide) as the

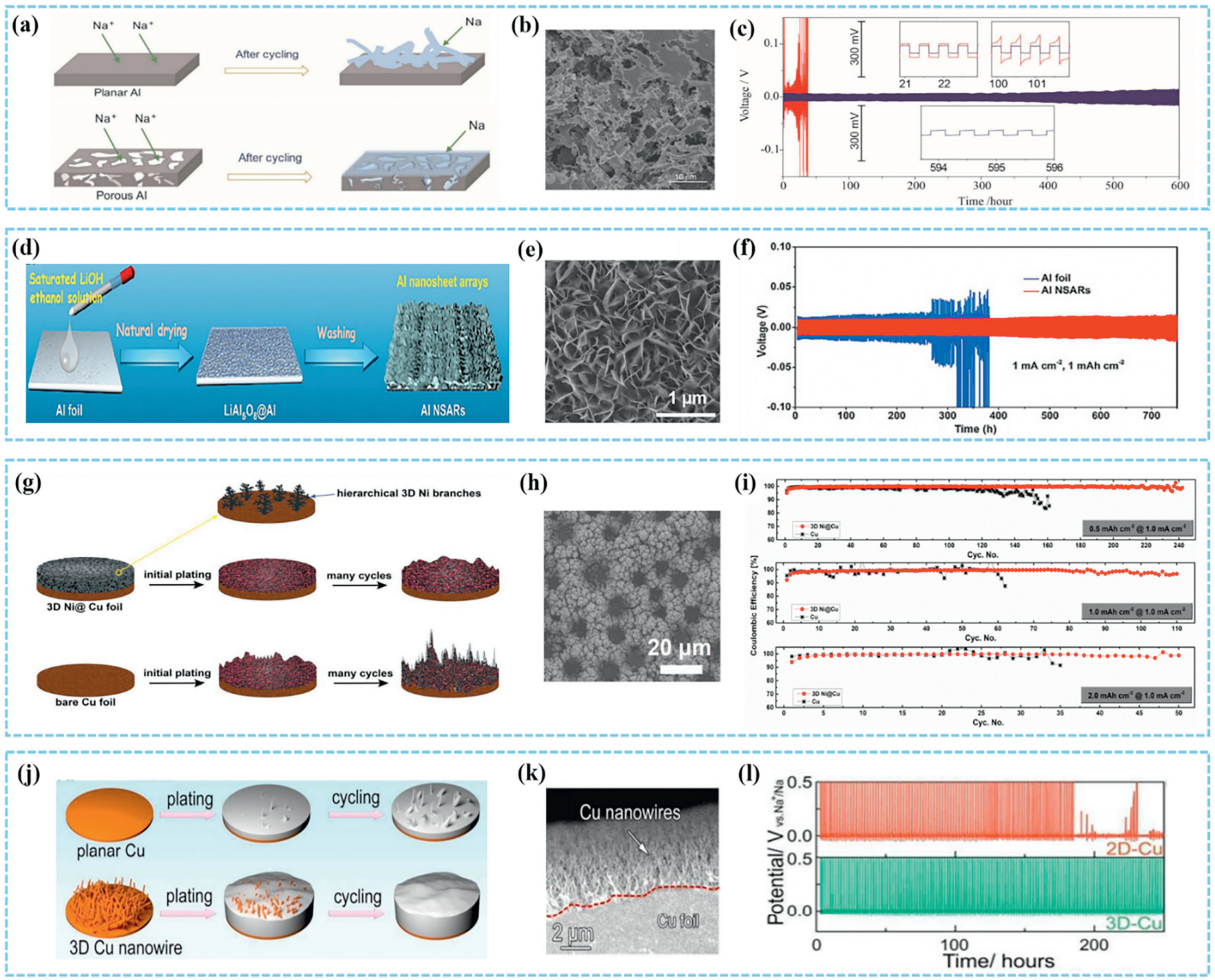

Fig. 3. (a) Schematic illustration of Na plating. (b) SEM image of porous Al. (c) Voltage profiles for Na plating and striping at 0.25 mA/cm^2. Reproduced with permission [73]. Copyright 2017, American Chemical Society. (d) Schematic diagram for the preparation of Al NSARs and (e) SEM image. (f) Cycling performance of symmetrical cells at 1 mA/cm^2 and 1 mAh/cm^2. Reproduced with permission [74]. Copyright 2022, Elsevier. (g) Schematic illustration of Na plating and (h) SEM image of 3D Ni@Cu. (i) CE of different current collectors. Reproduced with permission [75]. Copyright 2018, Elsevier. (j) Schematics of Na plating and (k) SEM image of Cu nanowires. (l) Cycling performance at 0.5 mA/cm^2. Reproduced with permission [77]. Copyright 2017, The Royal Society of Chemistry.

shell and copper as the core [79]. The Cu foam that has undergone surface treatment exhibits better wettability with molten sodium. In addition, Liu *et al.* uniformly and vertically grew Cu_2Se nanosheets with a thickness of about 55 nm on the surface of a copper skeleton [80]. The functional composite Na anode (Na_2Se/Cu@Na) was obtained by immersing the modified current collector into molten Na at a temperature of 300 °C through the spontaneous reaction and siphoning effect between Cu_2Se nanosheets and molten Na (Fig. 4a). The average Young's modulus value of Na_2Se/Cu@Na obtained using atomic force microscopy (AFM) was 8.8 GPa, which was higher than that of the bare Na anode (3.1 GPa). Composite electrodes with high interfacial stability and high conductivity have faster electrode reaction kinetics, which facilitates the redistribution of ion concentration and induces uniform nucleation of sodium (Figs. 4b and c).

Wang and coworkers uniformly grew copper nanowires with a length of tens of microns *in-situ* along the direction of the 3D Cu foam skeleton (CuNW-Cu) [81]. The thickness of the composite current collector is estimated at 250 μm (Fig. 4d). Depending on the synergistic effect between Cu nanowires and porous Cu foam, sodium deposition would be limited to the nanowire-enhanced area, significantly impeding the expansion of sodium dendrites (Fig. 4e). The cells could be plated/stripped on CuNW-Cu for more than 1400 h at a current density of 1 mA/cm^2 and a fixed area capacity of 2 mAh/cm^2 with an average voltage hysteresis ~25 mV (Fig. 4f). By utilizing FeS_2 as the cathode, Na@CuNW-Cu as the anode, and 1 mol/L $NaPF_6$ in diglyme as the electrolyte, the full cell achieved a high energy density of ~442 Wh/kg based on the mass of the cathode and anode materials.

Jiang *et al.* modified 3D porous nickel foam decorated by arrays of Fe_2O_3 nanosheets (Fe_2O_3@Ni) using a simple solution reaction (Fig. 4g) [82]. Notably, the sodiophilic nature of Fe_2O_3 contributes to reducing the nuclear barrier of Na, while the 3D mesh structure of the nickel foam provides a conductive network and space for Na deposition. This synergistic effect promotes the uniform deposition of Na and inhibits the formation of Na dendrites, which in turn improves the cycle life of the cell (Fig. 4h). The experimental results showed that Fe_2O_3@Ni exhibited an ultra-stable plating/stripping behavior with high CE (99.77%) after 1000 cycles (or 4000 h) at a current density of 0.5 mA/cm^2. Ultra-low voltage polarization (25 mV) and long cycle life (500 h) were achieved in the symmetric battery at 5 mA/cm^2 and 1 mAh/cm^2 (Fig. 4i). In addition, the full cell equipped with Na/Fe_2O_3@Ni as anode and NVP as cathode was able to maintain a capacity of 97.9 mAh/g after 500 cycles at 5 C.

In addition, Sun *et al.* successfully prepared Cu/Cu_2O modified Ni foam (CNF) by displacement reaction in a water bath [83]. The CNF features excellent mechanical ductility and a 3D porous core-

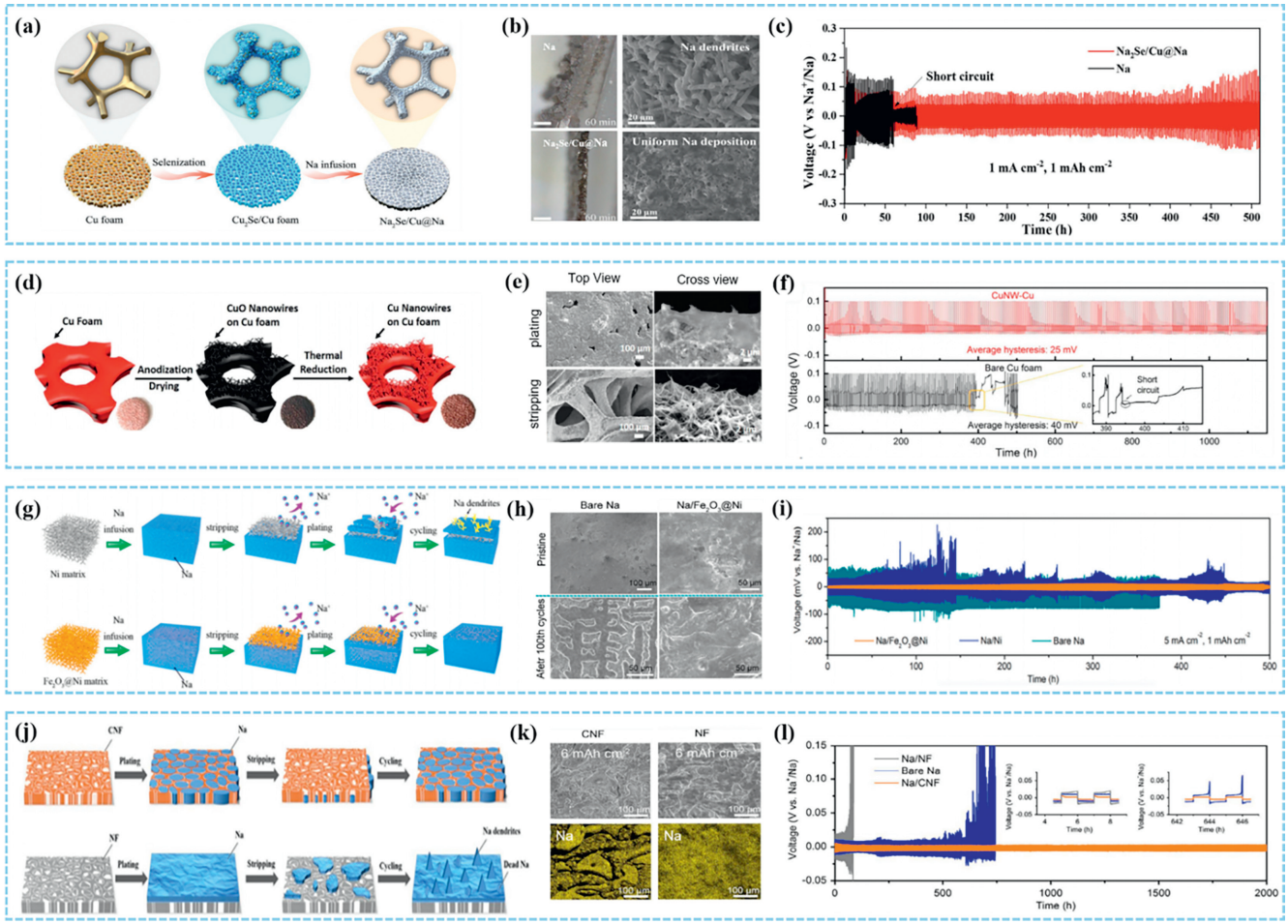

Fig. 4. (a) The illustration of the synthesis process of Na_2Se/Cu@Na. (b) The *in situ* optical microscopy of bare Na and composite Na anode at 1 mA/cm^2 and the corresponding surface morphology after the plating process. (c) Voltage profiles for Na plating and striping at 1 mA/cm^2 and 1 mAh/cm^2. Reproduced with permission [80]. Copyright 2022, Wiley-VCH GmbH. (d) Schematic illustration for the preparation process of Cu nanowires *in-situ* grown on Cu foam. (e) Morphological evolution during the Na plating and stripping on CuNW-Cu. (f) Voltage profiles of Na plating/stripping on different current collectors. Reproduced with permission [81]. Copyright 2018, Elsevier. (g) Schematic diagram of the metallic Na plating/stripping on different current collectors. (h) SEM images of different electrodes at 1 mA/cm^2 and 1 mAh/cm^2. (i) Voltage profiles of Na plating/stripping on different current collectors. Reproduced with permission [82]. Copyright 2022, Elsevier. (j) Schematic illustration of the metallic Na plating/stripping. (k) SEM images and corresponding EDS mapping characterization of Na depositing on CNF and NF with 6 mAh/cm^2. (l) Voltage-time profiles of the Na plating/stripping process in symmetrical cells. Reproduced with permission [83]. Copyright 2020, Wiley-VCH Verlag GmbH & Co. KGaA, Weinheim.

shell columnar structure, which could serve as a stabilizing carrier to effectively regulate the nucleation process of dendrite-free Na anode (Fig. 4j). When the deposition of sodium metal starts, the Cu_2O loaded on the CNF reacts with the sodium metal to form Na_2O, which guides the uniform deposition of Na metal in the CNF skeleton and pores. Even with a deposition capacity of up to 6 mAh/cm^2, the Na metal remains confined within the porous structure of the CNF, thus avoiding the formation of dendrites (Fig. 4k). In contrast, unmodified Ni foam leads to sodium metal aggregation on the surface and eventual dendrite formation as the amount of sodium metal deposited increases. More importantly, the sodium anode with CNF matrix (Na/CNF) exhibited a lower voltage hysteresis (13 mV) and a longer cycle life (2000 h) under the cycling conditions with a current density of 1 mA/cm^2 and a cycling capacity of 1 mAh/cm^2 (Fig. 4l). In conclusion, the Na anodes prepared using CNF substrates exhibit excellent stability with excellent plating/stripping properties.

The stability of the long-term cycling performance of the Na metal anode could be achieved by adjusting the distribution of the pro-sodium sites and rationally designing the structure of the sodiophilic framework. However, excessive specific surface area and vacant spatial structure may lead to excessive electrolyte consumption, imprison the deposited sodium source, and reduce the energy density of the battery. Therefore, it is imperative to design more innovative 3D composite current collectors.

3.3. Multi-coordination towards functional MCCs

By optimal design of the surfaces of planar and 3D MCCs, the affinity of the substrate for sodium can be enhanced, thus guiding the sodium metal toward uniform deposition. However, it should be noted that the low transport resistance of the MCCs surface allows sodium to accumulate on its upper surface during long cycling processes. When facing high current density and high plating/striping capacity, inactive sodium is easily formed and dendrite growth is induced. Therefore, a rational design of multi-directional coordinated functional MCCs is necessary to optimize the sodium deposition route. Next, we concluded the strategies for building heterogeneous structures and introducing magnetic elements on MCCs surface to optimize sodium metal deposition behavior.

3.3.1. Constructing heterogeneous structures on MCCs surface

By rational structural design, it is possible to construct a composite skeleton with gradient sodiophilic properties to guide the

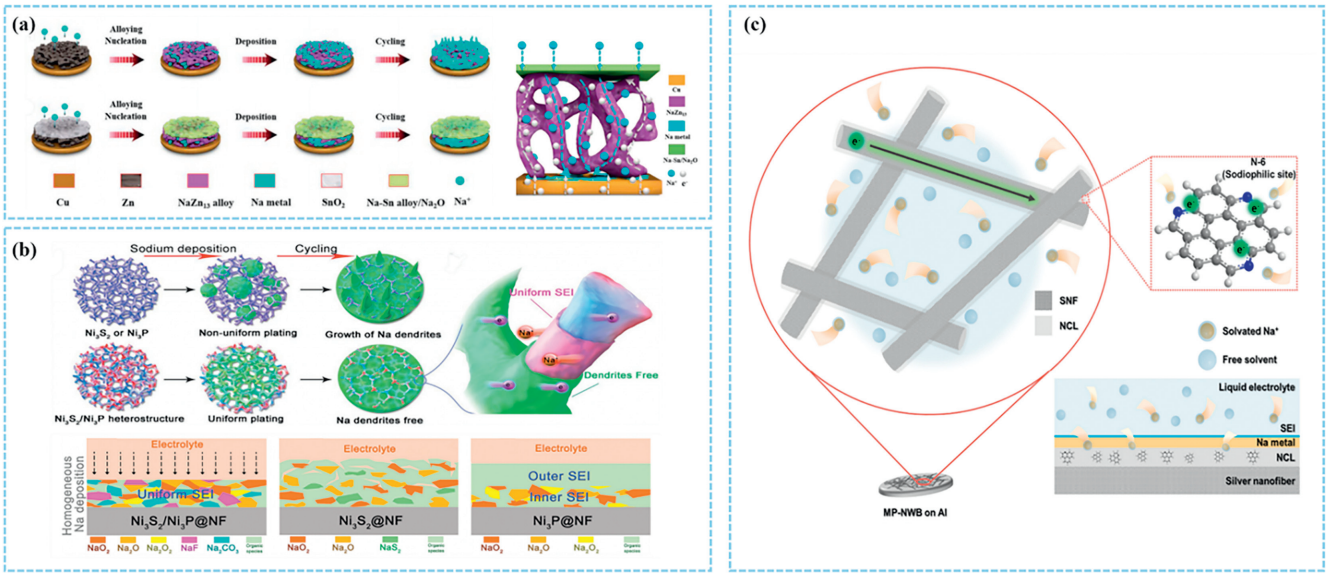

Fig. 5. (a) Schematic diagrams of deposition behaviors of Na^+ on different current collectors. Reproduced with permission [84]. Copyright 2020, Elsevier. (b) Schematic diagram of the important role of the Ni_3S_2/Ni_3P heterostructure for the formation of dendrite-free Na anode and the SEI components of different electrodes. Reproduced with permission [85]. Copyright 2023, Wiley-VCH GmbH. (c) Schematic diagram of the sodium metal storage behavior of MP-NWBs based on SNF@NCLs. Reproduced with permission [86]. Copyright 2019, Wiley-VCH Verlag GmbH & Co. KGaA, Weinheim.

bottom-up sodium deposition pattern, thus reducing the formation of dendrites and improving the utilization of the internal space of the skeleton. Chen's group introduced a porous sodiophilic Zn metal framework modified by a SnO_2 surface layer on Cu foil by magnetron sputtering, and the Zn/SnO_2 film showed a porous structure with a total thickness of about 600 nm [84]. The $Cu/Zn/SnO_2$ current collector transforms into a Cu/Na-Zn-Sn/Na_2O scaffold by the multi-step electrochemical reactions between Na^+ with Zn and SnO_2 (Fig. 5a). Compared to the *in-situ* induced Na_2O surface layer, the alloy-based skeleton has a higher ionic conductivity. The resulting potential gradient allows sodium ions to diffuse into the intercalation layer and gradually deposit within the skeleton. The $Cu/Zn/SnO_2$@Na symmetric cell exhibits excellent electrochemical performance and can be cycled for about 700 h even at a high current density of 5 mA/cm^2 with a total capacity of 5 mAh/cm^2.

In addition, Huang *et al.* synthesized Ni_3S_2/Ni_3P heterostructures on porous Ni foam by sintering, which can serve as a functional current collector scaffold for high-efficiency and dendrite-free SMAs [85]. Theoretical simulation calculations have shown that the heterostructure could enhance the spatial electron concentration of the Ni_3S_2/Ni_3P@NF@Na electrode and strengthen the adsorption energy for Na. Cryo-Transmission Electron Microscope (Cryo-TEM) images reveal that the Ni_3S_2/Ni_3P@NF@Na electrode has a uniform SEI with a thickness of only 25 nm. Moreover, titration gas chromatograph (TGC) measurement and X-ray photoelectron spectroscopy (XPS) analysis demonstrate that the ultrathin SEI has a characteristic "plum pudding" structure. Compared with other uneven and thick SEI structures, it could inhibit the further decomposition of electrolytes and promote the uniform Na^+ flux to achieve uniform Na plating (Fig. 5b). Assembling the functional current collector with sodium into a cell, it could cycle steadily for 700 cycles at a current density of 0.5 mA/cm^2 and a surface capacity of 0.5 mAh/cm^2, maintaining a high average CE of 99.3%. Full cell assembled with Ni_3S_2/Ni_3P@NF@Na electrode and NVP cathode offers an ultra-stable capacity of 81% even after 10,000 cycles at the high rate of 20 C.

Lee *et al.* successfully synthesized a silver nanofiber@nitrogen-rich carbon thin layer core-shell material (SNF@NCL) using the polyol method with low-temperature heating treatment [86]. Then, this material was uniformly deposited in the form of thin nanowebs on an Al current collector. Following a four-probe method, the macroporous nanowebs (MP-NWBs) constituted by SNF@NCL exhibited a high electronic conductivity of over 80 S/cm. The nanowebs possess a sodiophilic shell, which is capable of adsorbing sodium ions efficiently. At the same time, its solid conductive metal core not only transfers electrons, but also possesses excellent mechanical strength, thus ensuring the stability of the battery over long cycles (Fig. 5c). After 1600 cycles, the MP-NWBs recovered from the test cells were reassembled using the same configuration. Excitingly, the reassembled cell achieved an additional 1500 cycles, demonstrating a stable CE of up to 99.9%.

The construction of an artificial pro-sodium gradient or a functional composite heterostructure skeleton on the surface of the MCCs can effectively inhibit the formation of dendrites. Moreover, the design optimization of heterogeneous structures carries great potential for discovery and innovation owing to the constantly changing internal environment of the battery.

3.3.2. Introduction of magnetic elements

In recent years, a large number of studies have reported regulatory strategies for applying magnetic fields to battery systems [87,88]. Based on the synergistic effect of magnetic and electric fields, the growth of dendrites can be effectively suppressed and the electrochemical performance of batteries can be improved. Specifically, the magnetohydrodynamics (MHD) effect refers to the helical motion of charged particles in the electrolyte under the action of Lorentz forces perpendicular to the electric and magnetic fields when electrochemical processes are carried out under magnetic field, resulting in convection, which can effectively promote mass transfer and uniform distribution of ions [89].

In view of the above considerations, Shen's team proposed a simple method of applying a magnetic field to lithium metal anodes, and compared the ion deposition process with and without the magnetic field [88]. This strategy reduces the ion concentration gradient and polarization, achieving more stable electrode reactions and uniformly deposited metal layers. Wang's team proposed a strategy to suppress dendritic growth *via* the MHD effect [89]. The relationship between the deposition area radius and magnetic flux intensity was established by monitoring the deposition

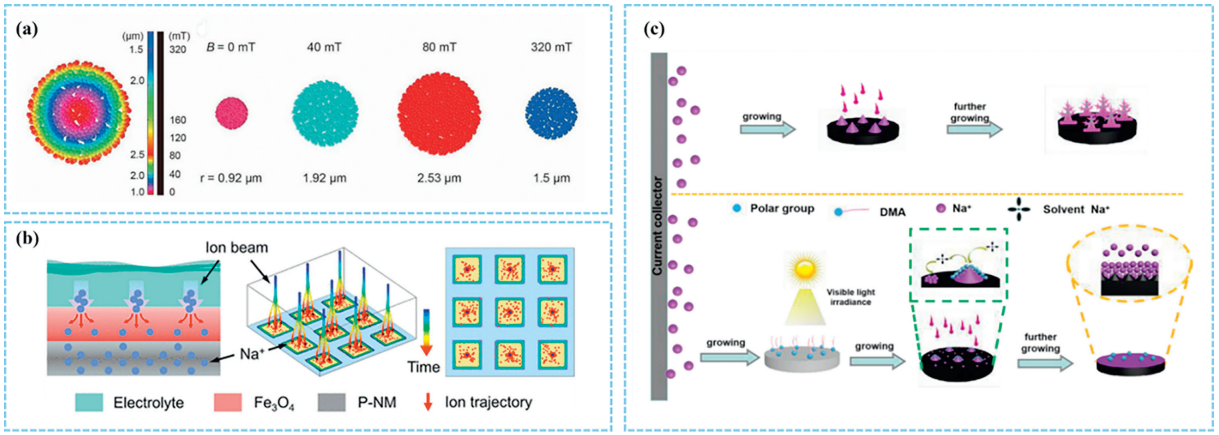

Fig. 6. (a) Finite element analysis using COMSOL Multiphysics showing the deposited area in the magnetic field from 0 to 320 mT. Reproduced with permission [89]. Copyright 2019, Wiley-VCH Verlag GmbH & Co. KGaA, Weinheim. (b) Schematic diagram of the trajectory of Na^+ diffusion during discharge with magnetic field and simulation results of different Na^+ trajectories upon diffusion process. Reproduced with permission [90]. Copyright 2023, American Chemical Society. (c) The schematic of the inhibited formation of dendrite sodium process *via* the generated electrostatic force due to sunlight. Reproduced with permission [91]. Copyright 2019, The Royal Society of Chemistry.

morphology and electrochemical performance (Fig. 6a), and this research conclusion was verified through the mathematical model and COMSOL Multiphysics simulation. By utilizing the magnetic field effect to inhibit the growth of dendrites, this approach can offer innovative solutions for optimizing and enhancing alkali metal batteries.

The enhancement of electrochemical processes by an external magnetic field usually occurs on several atomic layers near the electrode surface or interface, and in most cases, the magnetoelectric coupling is too weak to meet the demands of many practical applications. Sun's team designed and constructed a magnetic Fe_3O_4 interface layer on the surface of $Na_{2/3}Ni_{1/3}Mn_{2/3}O_2$, and coated the composites as an active material on the surface of Al foil to prepare electrodes [90]. By simulating the trajectories of ion diffusion with and without a magnetic field, they demonstrated that the phenomenon of Na ions flux gathering on the electrode surface is weakened in the presence of a magnetic field. Finite element calculations were conducted on COMSOL Multiphysics to simulate the motion of Na ions in three-dimensional space under the coupling effect of electric and magnetic fields, validating this theory (Fig. 6b).

In a photomagnetic-assisted technique, Liu *et al.* deposited a MoS_2 layer on a hollow conducting carbon material embedded with carbon quantum dots and doped Fe atoms ($Fe@C@CQD@MoS_2$) [91]. This composite electrode material is unique in that it bridges the link between sodium storage with solar and magnetic energy. A large number of photoelectrons can efficiently reduce the electrolyte to generate a sturdy SEI film; the involvement of MoS_2 improves the rate of electron transfer and further optimizes the electrochemical kinetics; and the heteroatomic doping of Fe atoms reduces the sodium absorption energy of the composite material. Under the synergistic effect of photoelectronic and MHD effects, this material inhibits the growth of sodium dendrites during deposition and exfoliation (Fig. 6c). It buffers volume deformation and promotes electrochemical reaction kinetics.

The construction of functional MCCs through multifaceted coordination, such as introducing magnetic elements could effectively regulate the ion concentration distribution and induce homogeneous nucleation. However, due to the complexity of the structure design and the uncertainty of the coordination of multifield coupling, these strategies are somewhat limited in the practical application of batteries. Therefore, the development of cost-effective new composite electrode materials with outstanding magnetic properties and high stability has become a research direction with great potential.

4. Summary and outlook

A summary of the electrochemical performance of the modified MCCs is provided in Table 2 [58,60,63,65-68,70,72-74,76,78,80-83,85,86,92-96]. In this review, we systematically discuss the research progress in recent years to enhance the performance of SMAs by optimizing MCCs. The initial research strategy involves scratch-coating and *in-situ* synthesizing protective layers on the surface of flat MCCs, which not only preserves the morphology of MCCs but also reduces the interfacial resistance between the electrode layer and MCCs, resulting in a diminished nucleation barrier of sodium. The second type of research aims to achieve a larger specific surface area and more active sites for sodium ions to nucleate by the 3D structural design of flat MCCs and surface optimization of 3D MCCs, effectively inducing uniform deposition of sodium. The third type of research involves regulating the distribution path of ion flux on the electrode by means of functional modification for uniform dispersion of ions, thus suppressing the growth of dendrites and improving the electrochemical stability of the battery.

However, with the diversity of battery systems, there is a notable absence of comprehensive theoretical validation and experimental studies on MCCs. Therefore, the subsequent research emphasis could be concentrated on the following aspects:

(1) Investigating the potential mechanisms of Na dendrite nucleation and growth.
Various strategies have been adopted to modify the MCCs with the aim of inhibiting the growth of sodium dendrites. Despite the positive effects of these strategies, the mechanisms of sodium dendrite formation and growth remain to be fully revealed. Hence, there is a pressing need to reinforce pertinent theoretical research in the foreseeable future. In-depth analyses combining *in-situ* and *ex-situ* advanced characterization techniques are expected to be carried out to uncover the potential connection between cell configuration and sodium dendrite nucleation/growth mechanism. By doing so, we can investigate more appropriate MCC materials for application in SMBs.

(2) Exploring more efficient modification methods.
The introduction of coating materials and sodium-friendly alloy layers on the MCCs surface can indeed reduce the nu-

Table 2
Comparison of electrochemical performance of SMBs with differently modified MCCs.

Modified MCC	Electrolyte	Half-cell performance (current density [mA/cm^2], areal capacity [mAh/cm^2], lifespan, average CE [%])	Symmetry-cell performance (current density [mA/cm^2], areal capacity [mAh/cm^2], lifespan)	Full-cell performance (cathode, rate performance, lifespan)	"Anode-free" full cell performance (cathode, rate performance, lifespan)	Ref.
Carbon/Al	1 mol/L $NaPF_6$ in diglyme	0.5, 0.25, 1000 n, 99.8	–	–	FeS_2, 0.125 mA/cm^2, 40 n	[58]
F-A-Al	Homemade ionic liquid electrolyte	–	0.5, 0.5, 600 h	–	NVP, 0.3 C, 50 n	[65]
Porous Al	1 mol/L $NaPF_6$ in diglyme, 1 mol/L $NaClO_4$ in EC/DEC	1, 0.5, 1000 n, 99.8	0.5, 0.25, 1000 h	NVP, 0.1 mA/cm^2, 375 n	TiS_2, 0.1 mA/cm^2, 200 n	[73]
Al NSARs	1 mol/L $NaPF_6$ in DME	2, 2, 650 n, 99.99	1, 1, 750 h	NVP, 20 C, 1800 n	–	[74]
3D Zn@Al	1 mol/L $NaPF_6$ in DME	2, 2, 500 n, 99.5	1, 1, 1500 h	NVP, 5 C, 2000 n	NVP, 0.5 C, 100 n	[76]
NaHFAl	1 mol/L $NaClO_4$ in EC/PC+5%FEC	–	1, 1, >400 h	SPAN, 0.5 C, 800 n	–	[78]
MP-NWBs on Al	1 mol/L $NaPF_6$ in diglyme	1, 0.5, 1600 n, >99.9	–	–	$Na_{1.5}VPO_{4.8}F_{0.7}$, 0.1 A/g, 100 n	[86]
Fe-MCN@Cu	1 mol/L $NaPF_6$ in diglyme	1, 1, 850 n, 99.97	1, 1, 2600 h	NVP, 1 C, 2000 n	–	[60]
PSN@Cu	1 mol/L $NaPF_6$ in diglyme	2, 2, 1400 n, 99.73	1, 1, 2300 h	FeS_2, 0.2 A/g, 100 n	–	[63]
CuP_2@Cu	1 mol/L $NaPF_6$ in diglyme	2, 2, 420 n, 99.71	1, 2, 1200 h	$NaTi_2(PO_4)_3$, 5 C, 800 n	–	[66]
HCOONa-Cu	1 mol/L $NaPF_6$ in diglyme	–	2, 1, 2200 h	NVP, 2 C, 800 n	NVP, 0.5 C, 400 n	[67]
Cu@Au	1 mol/L $NaSO_3CF_3$ in diglyme	1, 1, 300 n, 99.8	–	–	FeS_2, charge 0.1 A/g, discharge 1 A/g, 50 n	[68]
Cu_6Sn_5@Cu	1 mol/L $NaPF_6$ in diglyme	5, 1, 2000 n, 99.83	2, 2, 2000 h	FeS_2, 0.2 A/g, 1500 n	–	[70]
Bi⊂CNs@Cu	1 mol/L $NaSO_3CF_3$ in diglyme, 1 mol/L $NaClO_4$ in EC/PC + 5%FEC	1, 3, 1287 n, 99.92	1, 1, 4000 h	Prussian blue, 1 C, 290 n	–	[72]
Na_2Se/Cu	1 mol/L $NaClO_4$ in EC/DEC + 5%FEC	–	1, 1, >500 h	NVP, 10 C, >800 n	–	[80]
CuNW-Cu	1 mol/L $NaPF_6$ in DME	1, 2, >350 n, 99.7	1, 1, 500 h	FeS_2, 0.2 A/g, 50 n	–	[81]
PC-CFe on Cu	1 mol/L $NaPF_6$ in diglyme	4, 8, 1200 n, 99.8	5, 5, >1600 h	NVPF, 0.55 mA/cm^2, 500 n	NVP, 1 mA/cm^2, 100 n	[92]
Pt-Cu foam	1 mol/L $NaSO_3CF_3$ in diglyme, 1 mol/L $NaPF_6$ in EC/DMC + FEC	0.5, 0.5, 200 n, 97	0.5, 0.5, 320	Cu_2Se, 0.1 A/g, >500 n	–	[93]
CF@ZnO	1 mol/L $NaSO_3CF_3$ in diglyme	1, 1, 300 n, 99.6	1, 1, 350 h	NVP, 10 C, 500 n	–	[94]
Bi@Cu	1 mol/L $NaPF_6$ in DME	2, 1, 750 n, 99.6	–	NVP, 1 C, 80 n	–	[95]
Fe_2O_3@Ni	1 mol/L $NaPF_6$ in diglyme	1, 1, 1000 n, 99.75	5, 1, 500 h	NVP, 5 C, 500 n	–	[82]
CNF	1 mol/L $NaPF_6$ in diglyme	1, 1, 400 n, -	1, 1, 2000 h	NVP, 5 C, 300 n	–	[83]
Ni_3S_2/Ni_3P@NF	1 mol/L $NaClO_4$ in EC/DEC + 5%FEC, 1 mol/L $NaPF_6$ in DME	0.5, 0.5, >700 n, 99.3	5, 5, 5000 h	NVP, 20 C, 10,000 n	–	[85]
NG-NF	1 mol/L $NaPF_6$ in diglyme	0.5, 1, 800 n, >99	1, 1, 1000 h	NVP, 2 C, 250 n	–	[96]

DME: 1,2-dimethoxyethane; EC: ethylene carbonate; PC: propylene carbonate; FEC: fluoroethylene carbonate; DEC: diethyl carbonate; DMC: dimethyl carbonate; SPAN: sulfurized polyacrylonitril; NVP: $Na_3V_2(PO_4)_3$; NVPF: $Na_3V_2(PO_4)_2F_3$.

cleation barrier of sodium. However, the selection of suitable coating materials and the optimization of the preparation process still need to be further explored. In addition, repeated alloying/dealloying during long-term cycling may result in the rupture and exfoliation of the sodiophilic layer. Introducing 3D skeletons with strong ionic conductivity and high specific surface area in the surface modification process of MCCs is a promising research strategy. However, an excessively large specific surface area and spatial structure will diminish the utilization of active materials and harm the battery efficiency. Therefore, it is imperative to devise more innovative and comprehensive structural designs that optimize the spatial distribution arrangement of the sodiophilic materials, to enhance the electrochemical performance of SMAs.

(3) Designing modified current collectors suitable for AFSMBs.
The lack of an additional source of sodium for AFSMBs makes the sodium contained in the cathode particularly valuable. The modified current collector designed for such batteries should equipped with two core functions: firstly, it is supposed to be capable of accommodating the volume expansion of the cell induced by the deposited sodium metal. Secondly, it should be ensured that the sodium metal achieves a reversible plating/stripping process with high CE on the current collector. The meticulous design of the current collector with its unique structure should be able to perfectly match the cathode capacity and efficiently store a reversible source of sodium. This innovative modification not only significantly reduces the irreversible loss of sodium, but also greatly inhibits the expansion of the battery volume. We strongly expect that this promising current collector modification pathway will provide a great impetus to the advancement of SMBs with high-weight energy density and high-volumetric energy density.

(4) Engineering magnetic composite electrode materials.
To tackle the obstacles in applying magnetic fields to SMBs, it is imperative to investigate the interplay between magnetic field intensity and materials. Simultaneously, a study is needed to rationally position the magnetic field without compromising the energy density of the battery. To attain the aforementioned objectives, efforts may be taken to develop new composite electrode materials that are cost-effective and possess outstanding magnetic properties and high stability, thereby enhancing the cycling performance and energy density of batteries. This research direction holds significant potential and warrants further investigation and exploration.

(5) Theoretical simulation and experimental verification.
By combining theoretical simulation with experimental validation, researchers can delve deeper into the dispersion mechanism of the surface ion flux in modified MCCs. It provides profound theoretical guidance and experimental support for the precise regulation of sodium ion nucleation. COMSOL Multiphysics simulation, TGC measurement, *in-situ* transmission electron microscopy (TEM), mass spectrometry, and scanning transmission X-ray microscopy (STXM) can serve as characterization tools to provide a more intuitive explanation of the reaction mechanism inside the cell.

In conclusion, despite the considerable distance that remains before we attain high-performance MCCs, our ongoing research into the synergistic effects of various optimization systems gives us hope that stabilized and commercialized modified MCCs are within reach and will make a significant impact on the future of next-generation battery energy storage.

Declaration of competing interest

The authors declare that they have no known competing financial interests or personal relationships that could have appeared to influence the work reported in this paper.

CRediT authorship contribution statement

Zhenyang Yu: Writing – review & editing. **Yueyue Gu:** Writing – original draft. **Qi Sun:** Data curation. **Yang Zheng:** Resources. **Yifang Zhang:** Writing – review & editing. **Mengmeng Zhang:** Resources. **Delin Zhang:** Funding acquisition. **Zhijia Zhang:** Writing – review & editing. **Yong Jiang:** Supervision.

Acknowledgments

This study was financially supported by the National Natural Science Foundation of China (Nos. 52102291, 52271011, and 51701142) and was also supported by a grant from the Cangzhou Institute of Tiangong University (No. TGCYY-F-0201).

References

[1] J.J. Long, H. Yu, W.B. Liu, Rare Met. 43 (2024) 1370–1389.
[2] H. Li, S.H. Chang, M.M. Zhang, Copper Eng. 6 (2023) 38–50.
[3] Y. Niu, Y. Zhao, M. Xu, Carbon Neut. 2 (2023) 150–168.
[4] Y. Ouyang, W. Zong, J. Wang, et al., Energy Storage Mater. 42 (2021) 68–77.
[5] C. Ding, L. Huang, J. Lan, et al., Small 16 (2020) e1906883.
[6] L.J. Xie, C. Tang, Z.H. Bi, et al., Adv. Energy Mater. 11 (2021) 2101650.
[7] H. Kim, J.C. Hyun, D.H. Kim, et al., Adv. Mater. 35 (2023) e2209128.
[8] Y.Y. Guo, Y.H. Cao, J.D. Lu, et al., Microstructures 3 (2023) 2023038.
[9] M.Q. Gao, W.Y. Zhou, Y.X. Mo, et al., Adv. Fiber Mater. 1 (2022) 100006.
[10] Y. Zhang, W.Y. Wang, Y.P. Wang, et al., Copper Eng. 4 (2023) 23–31.
[11] Q. Yang, Q. Fan, J. Peng, et al., Microstructures 3 (2023) 2023013.
[12] D.Q. Liu, J. Shen, Z.Z. Jian, et al., Energy Mater. 3 (2023) 300028.
[13] Z.Q. Zhao, X.Y. Zhao, Y.M. Zhou, et al., Adv. Powder Mater. 2 (2023) 100139.
[14] Z.J. Zhang, J.P. Guo, S.H. Sun, et al., Rare Met. 42 (2023) 3607–3613.
[15] C. Li, H. Xu, L. Ni, et al., Adv. Energy Mater. 13 (2023) 2301758.
[16] K.C. Pu, X. Zhang, X.L. Qu, et al., Rare Met. 39 (2020) 616–635.
[17] F.Y. Shi, C.H. Chen, Z.L. Xu, Adv. Fiber Mater. 3 (2021) 275–301.
[18] Z.L. Li, T.T. Liu, C.Q. Duan, et al., Copper Eng. 4 (2023) 1–13.
[19] Y. Zhao, W. Cheng, J.H. Wu, et al., Chin. Chem Lett. 34 (2023) 107413.
[20] J. Xu, J. Yang, Y. Qiu, et al., Nano Res. 17 (2024) 1288–1312.
[21] T.Y. Song, C.C. Wang, C.S. Lee, Carbon Neut. 1 (2022) 68–92.
[22] T. Li, H. Liu, P. Shi, et al., Rare Met. 37 (2018) 449–458.
[23] J.Y. Hu, H.W. Wang, S.W. Wang, et al., Energy Storage Mater. 36 (2021) 91–98.
[24] Q. Ni, Y.J. Yang, H.S. Du, et al., Batteries 8 (2022) 272.
[25] P. Molaiyan, M. Abdollahifar, B. Boz, et al., Adv. Funct. Mater. 34 (2024) 2311301.
[26] C.Y. Zhang, A.X. Wang, J.H. Zhang, et al., Adv. Energy Mater. 8 (2018) 1802833.
[27] B.L. Wu, C.G. Chen, L.H.J. Raijmakers, et al., Energy Storage Mater. 57 (2023) 508–539.
[28] H. Wang, E. Matios, J. Luo, et al., Chem. Soc. Rev. 49 (2020) 3783–3805.
[29] B. Qin, Y. Ma, C. Li, et al., Energy Storage Mater. 61 (2023) 102891.
[30] J. Lee, Y. Lee, J. Lee, et al., ACS Appl. Mater. Interface 9 (2017) 3723–3732.
[31] L. Yang, J.W. Chen, S. Park, et al., Energy Mater. 3 (2023) 300042.
[32] Z.G. Tian, Y.G. Zou, G. Liu, et al., Adv. Sci. 9 (2022) 2201207.
[33] W. Fang, R. Jiang, H. Zheng, et al., Rare Met. 40 (2020) 433–439.
[34] M. Moorthy, B. Moorthy, B.K. Ganesan, et al., Adv. Funct. Mater. 33 (2023) 2300135.
[35] S.Z. You, M.H. Ye, J.M. Xiong, et al., Small 17 (2021) 2102400.
[36] Y. Deng, J.X. Zheng, Q. Zhao, et al., Small 18 (2022) 2203409.
[37] J. Chen, Y. Wang, S. Li, et al., Adv. Sci. 10 (2022) e2205695.
[38] P.C. Liu, Y.X. Wang, H.C. Hao, et al., Adv. Mater. 32 (2020) 2002908.
[39] H. Jeong, J. Jang, C. Jo, Chem. Eng. J. 446 (2022) 136860.
[40] X. Li, M. Zhao, Q. Guo, et al., J. Mater. Sci. Technol. 176 (2024) 112–118.
[41] Y. Liu, Y. Xu, J. Wang, et al., Mater. Today Sustain. 18 (2022) 100127.
[42] W. Xu, Y. Li, J. Yao, et al., J. Appl. Electrochem. 53 (2023) 1953–1957.
[43] Z.J. Zhang, S.H. Sun, Y.F. Chen, et al., Chin. Chem. Lett. 35 (2024) 108922.
[44] X. Li, S. Deng, M.N. Banis, et al., ACS Appl. Mater. Interfaces 11 (2019) 32826–32832.
[45] C.X. Han, G.S. Chen, Y. Ma, et al., Energy Mater. 3 (2023) 300052.
[46] Z.K. Zhou, Q. Chen, Y. Wang, et al., Batteries 9 (2023) 188–204.
[47] L.F. Zhang, Y.H. Xia, H. Yang, et al., APL Mater. 10 (2022) 070901.
[48] M.Z. Wang, M. Tang, S.L. Chen, et al., Adv. Mater. 29 (2017) 1703882.
[49] T.E. Fan, H.F. Xie, J. Alloys Compd. 775 (2019) 549–553.
[50] X.M. Xia, C.F. Du, S. Zhong, et al., Adv. Funct. Mater. 32 (2021) 2110280.
[51] Y.W. Yao, X.X. Wang, C.L. Dong, et al., J. Power Source. 523 (2022) 231034.
[52] Z.C. Shen, J.W. Zhong, J.H. Chen, et al., Chin. Chem Lett. 34 (2023) 107370.
[53] S. Byun, J. Yu, J. Power Source. 307 (2016) 849–855.

[54] S. Jeong, V.C. Ho, O. Kwon, et al., Energy Mater. 3 (2023) 300048.
[55] C.L. Wei, L.W. Tan, Y.C. Zhang, et al., J. Mater. Sci. Technol. 115 (2022) 156–165.
[56] K.W. Apurva Patrike, M.V. Shelke, Chem. Asian J. 18 (2023) 2300068.
[57] Y. Li, Q. Zhou, S. Weng, et al., Nat. Energy 7 (2022) 511–519.
[58] A.P. Cohn, N. Muralidharan, R. Carter, et al., Nano Lett. 17 (2017) 1296–1301.
[59] O.J. Dahunsi, B. Li, B. An, et al., Energy Fuel. 37 (2023) 7522–7529.
[60] C. Wei, G.X. Huang, J.Y. Mao, et al., ACS Appl. Energy Mater. 5 (2022) 10446–10456.
[61] H.H. Li, H. Zhang, F.L. Wu, et al., Adv. Energy Mater. 12 (2022) 2202293.
[62] Z. Hou, W.H. Wang, Y.K. Yu, et al., Energy Storage Mater. 24 (2020) 588–593.
[63] Q.W. Chen, Z. Hou, Z.Z. Sun, et al., ACS Appl. Energy Mater. 3 (2020) 2900–2906.
[64] S.Y. Wang, Y.L. Jie, Z.H. Sun, et al., ACS Appl. Energy Mater. 3 (2020) 8688–8694.
[65] S. Wu, J. Hwang, K. Matsumoto, et al., Adv. Energy Mater. 13 (2023) 2302468.
[66] X.L. Zhu, Y. Wang, W.Y. Wang, et al., Chem. Eng. J. 446 (2022) 136917.
[67] C.Z. Wang, Y. Zheng, Z.N. Chen, et al., Adv. Energy Mater. 13 (2023) 2370094.
[68] S. Tang, Z. Qiu, X.Y. Wang, et al., Nano Energy 48 (2018) 101–106.
[69] S. Tang, Y.Y. Zhang, X.G. Zhang, et al., Adv. Mater. 31 (2019) 1807495.
[70] Q.W. Chen, T.X. Zhang, Z. Hou, et al., Chem. Eng. J. 433 (2022) 133270.
[71] Y.F. Zhang, Q.W. Shi, Y.R. Zhong, et al., Sci. China Chem. 63 (2020) 1557–1562.
[72] L. Zhang, X.L. Zhu, G.Y. Wang, et al., Small 17 (2021) 2007578.
[73] S. Liu, S. Tang, X.Y. Zhang, et al., Nano Lett. 17 (2017) 5862–5868.
[74] F. Tang, R.Q. Xia, D. Chen, et al., J. Energy Chem. 74 (2022) 1–7.
[75] Y.L. Xu, A.S. Menon, P.P.R.M.L. Harks, et al., Energy Storage Mater. 12 (2018) 69–78.
[76] Z.J. Cai, F. Tang, Y. Yang, et al., Nano Energy 116 (2023) 108814.
[77] Y.Y. Lu, Q. Zhang, M. Han, et al., Chem. Commun. 53 (2017) 12910–12913.
[78] Y. Shuai, Y.L. Hu, J. Lou, et al., J. Electrochem. Soc. 170 (2023) 030519.
[79] C.L. Wang, H. Wang, E. Matios, et al., Adv. Funct. Mater. 28 (2018) 1802282.
[80] F.F. Liu, L.F. Wang, F.X. Ling, et al., Adv. Funct. Mater. 32 (2022) 2210166.
[81] T.S. Wang, Y.C. Liu, Y.X. Lu, et al., Energy Storage Mater. 15 (2018) 274–281.
[82] F.Y. Jiang, X.J. Li, J.H. Wang, et al., J. Alloys Compd. 910 (2022) 164762.
[83] J.C. Sun, M. Zhang, P. Ju, et al., Energy Technol. 8 (2020) 1901250.
[84] Q.L. Chen, B. Liu, L. Zhang, et al., Chem. Eng. J. 404 (2021) 126469.
[85] H.J. Huang, Y.L. Wang, M. Li, et al., Adv. Mater. 35 (2023) 2210826.
[86] M.E. Lee, S. Lee, J. Choi, et al., Small 15 (2019) 1901274.
[87] K. Shen, X.J. Xu, Y.P. Tang, Nano Energy 92 (2022) 106703.
[88] K. Shen, Z. Wang, X.X. Bi, et al., Adv. Energy Mater. 9 (2019) 1900260.
[89] A.X. Wang, Q.B. Deng, L.J. Deng, et al., Adv. Funct. Mater. 29 (2019) 1902630.
[90] S.W. Sun, X.N. Li, L.Q. Yan, et al., ACS Energy Lett. 8 (2023) 4349–4356.
[91] F.S. Liu, Y.Y. Xiao, P.Y. Han, et al., Nanoscale 11 (2019) 21081–21092.
[92] K. Lee, Y.J. Lee, M.J. Lee, et al., Adv Mater. 34 (2022) e2109767.
[93] J.Y. Wang, Q. Kang, J.C. Yuan, et al., Carbon Energy 3 (2021) 153–166.
[94] W. Yang, W. Yang, L.B. Dong, et al., Nano Energy 80 (2021) 105563.
[95] X.L. Cheng, D.J. Li, S. Peng, et al., Batteries 9 (2023) 408.
[96] C. Bao, B. Wang, Y. Xie, et al., ACS Sustain. Chem. Eng. 8 (2020) 5452–5463.